SF2A 2024
M. Béthermin, K. Baillié, N. Lagarde, J. Malzac, R.-M. Ouazzani, J. Richard, O. Venot, A. Siebert (eds)

FORMATION REGIONS OF CM AND CI CHONDRITES: SATURN VERSUS THE PRIMORDIAL TRANS-URANIAN DISK

S. Anderson[1], P. Vernazza[1] and M. Brož[2]

Abstract. The Solar System's current compositional distribution does not reflect the primordial disk's original makeup, due to dynamical reshuffling over 4.5 billion years. Understanding the provenance of the most primitive materials in our meteorite collections (CI and CM chondrites) is important not only for our comprehension of the Solar System's early evolution but also to provide the context of recent sample return missions. Today, there is a general consensus that these materials originate from beyond Jupiter based on isotopic measurements, but their respective formation locations remain elusive. Here, we show that the parent bodies of these two meteorite groups have distinct distributions in the asteroid belt, indicating either two distinct formation areas or two distinct formation times. We then use N-body simulations to simulate the effect of giant planet growth and migration to investigate the dynamical evolution of small bodies formed beyond Jupiter and up to Neptune when gas was still present in the disk ($\leq$5 Myrs after CAIs). We find that pressure bumps in the disk predominantly trap planetesimals irrespective of their formation zone, resulting in the gas disk profile entirely governing the radial distribution of implanted bodies in the asteroid belt. CI and CM-like bodies must have been implanted at different times in the belt whereas CI and comet-like bodies were implanted simultaneously, as the correlation between these two distributions has a $P > 0.05$. CM-like bodies were likely implanted during Saturn's growth whereas CI and comet-like bodies were likely implanted from the region beyond Uranus at a later stage, during the outward migration of Uranus and Neptune. A byproduct of our simulations is that CM-like bodies contributed to the water budget of the formation region of telluric planets. Our findings also underscore the influence of gas properties and the growth of giant planets on the system's evolution, which leads to biases in dynamical models.

Keywords: asteroids, chondrites, small body dynamics, solar system formation

1 Context

To date, the vast majority of meteorites ($\geq$99%) originate from asteroids in orbits between Mars and Jupiter, yet reaching a consensus on how their diverse chemical, compositional, and isotopic characteristics align with an in-situ formation model within the asteroid belt remains elusive. Recent dynamical models, leveraging measurements from carbonaceous chondrites (CCs), suggest that meteorites may originate from varied heliocentric distances, spanning from the terrestrial planet formation zone to the Kuiper Belt Morbidelli et al. (2005); Walsh et al. (2011); Raymond & Izidoro (2017). This broad range is evident in the distribution dichotomies among CCs, especially between CM chondrites (Ch, Cgh-types) and CI chondrites (B, C, Cb, and Cg-types), which collectively account for over 50% of the asteroid belt's mass, excluding Ceres Hopp et al. (2022); Yada et al. (2021); Yokoyama et al. (2023). These groups show distinctly different spatial distributions (Fig. 1): CM-like bodies display a Gaussian profile, whereas CI-like bodies show an asymmetric distribution, similar to comet-like P-type asteroids Vernazza et al. (2021). Our study aims to explore the formation and migration history of these asteroid types within the context of giant planet evolution and solar system dynamics to determine whether CM and CI chondrites originated from different locations or at different times — or both.

[1] Aix Marseille University, CNRS, CNES, LAM, Institut Origines, 38 rue Frédéric Joliot-Curie, Marseille, 13013,France
[2] Charles University, Faculty of Mathematics and Physics, Institute of Astronomy, V Holešovičkách 2, Praha, CZ-18200, Czech Republic

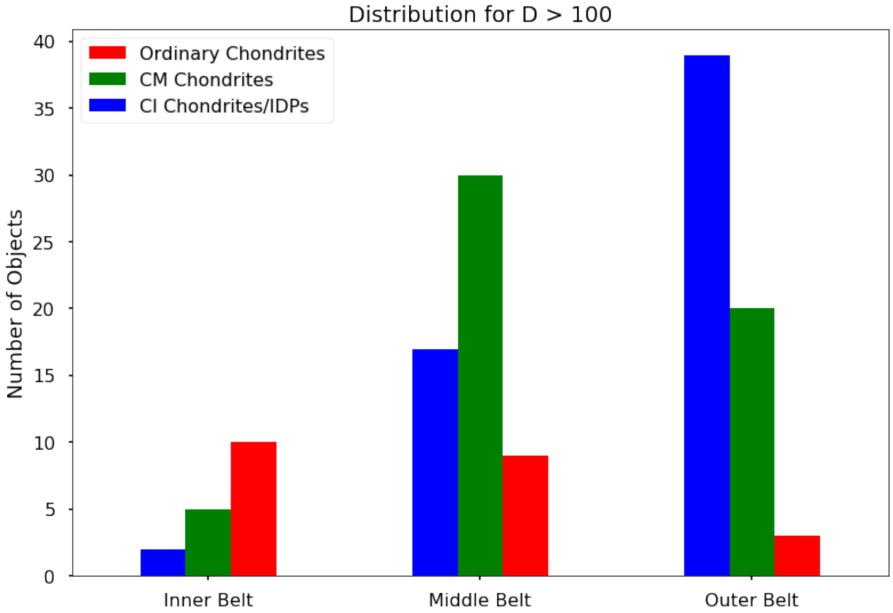

Fig. 1. Distribution of asteroids >100 km in Diameter in the asteroid belt. CM chondrites are more numerous in the middle belt while the CI chondrites/IDPs dominate in the outer belt. Ordinary Chondrites are more abundant in the inner belt.

2 Methods

We conducted simulations using the N-body integrator `REBOUND` (Rein & Liu 2012), each consisting of 20,000 test particles representing 100-km-sized planetesimals. Our five-planet model, motivated by Nesvorný (2015) and Deienno et al. (2017), featured Jupiter, Saturn, an additional ice giant (commonly ejected from the solar system), Uranus, and Neptune. As Jupiter grew to about $20M_{\oplus}$, it formed a pressure bump that isolated pebbles, opened a gap in the gas disk, and slowed its migration. This allowed planetesimals to form at the gap's edge, potentially leading to Saturn's core formation and the scattering of material toward Jupiter, which contributed to the formation of the asteroid belt, Galilean moons, and water delivery to terrestrial planets (Kobayashi et al. 2012; Lambrechts, M. et al. 2014). Initially, the planets were placed on low-eccentricity orbits, with Jupiter at 5.4 au and Saturn at 7.3 au at the edge of Jupiter's gap. We placed Neptune at two different locations, namely in a 'tight' configuration at 16.2 au, in a 3:2, 3:2, 3:2, 3:2 resonance chain, or in a 'wide' configuration at 20.3 au, in a 3:2, 3:2, 2:1, 3:2 resonance chain (Deienno et al. 2017). Jupiter was assumed to have reached its current mass ($\approx 300M_{\oplus}$) before the start of our simulations, while the remaining planetary cores started at $1M_{\oplus}$ and grew incrementally over timescales of $\tau_{\rm growth}$ ranging from 1×10^5 to 1×10^6 years. We chose to neglect the influence of telluric planets, which, having relatively small orbits, require more computation time. All planets interact with each other as well as the gas in the disk. We included orbital damping from gas interactions and accounted for aerodynamic drag, eccentricity, and inclination damping using a model already established by Ronnet et al. (2018) based on Cresswell & Nelson (2008).

Most of the small bodies of the outer Solar System originated from the region between Jupiter and ∼30 au Tsiganis et al. (2005); Gomes (2003); Levison et al. (2008); Kaib & Quinn (2008). Here, we are interested in the behavior of objects formed beyond Jupiter. With this in mind, we limit our simulations to planetesimals formed in the $7 < a < a_{\rm Neptune} + 1$ au range, where a is the initial semi-major axis of our test particles. Our model assigns an equal quantity of planetesimals across each semimajor axis segment, not to mirror the actual, unknown distribution but to ensure comprehensive coverage of potential source regions. Variations in the distribution of planetesimals would not significantly alter the likelihood of their implantation into the asteroid belt Raymond & Izidoro (2017), as interactions between planetesimals are minimal compared to those between planetesimals and planets or gas. The exact distribution of planetesimals is an interesting problem, as we know from observations of exosystems that a continuous disk at this stage is unlikely, and instead, we would have rings of planetesimals around the star resulting from the pressure bumps formed around ice lines and other condensation lines Izidoro et al. (2022). We accounted for the aerodynamic drag effects on the planetesimals

using the methods described by Ronnet et al. (2017); Ronnet et al. (2018).

We adopted a surface density profile $\Sigma_g \propto r^{-0.5}$ (Cresswell & Nelson 2008), normalized to $\Sigma_g = 300$ g/cm^2 at 1 au (Ronnet et al. 2018), consistent with a moderately evolved disk (Bitsch et al. 2015). We accounted for the gap formed by Jupiter by applying a Gaussian reduction in surface density around its orbit. The disk's turbulent viscosity was parametrized with $\alpha = 2 \times 10^{-3}$ (Shakura & Sunyaev 1973), and we tested values for low-viscosity disks as well. We also compared our chosen profile with those of Desch et al. (2018) and Raymond & Izidoro (2017), as their models were successful in implanting objects into the asteroid belt. A comparison of these profiles is shown in Fig. 2.

3 Results

Most parameters had a minor influence on implantation. Lower viscosity ($\alpha = 1 \times 10^{-4}$ vs. $\alpha = 2 \times 10^{-3}$) had little effect on the fit, likely because the particles were large enough to be partially decoupled from the gas. In contrast, faster planetary growth timescales accelerated planetesimal scattering, acting as a "speed dial" by clearing the surrounding space more quickly. However, neither longer ($\tau = 1 \times 10^6$ yr) nor shorter ($\tau = 1 \times 10^5$ yr) timescales significantly affected the final distribution of the planetesimals. Similarly, adjustments in gas quantity and scale affected implantation efficiency, with more gas speeding up orbital circularization.

In the absence of giant planet migration, over 90% of small bodies captured in the asteroid belt originate from the Saturn region ($a_{\rm ini} < 10$ au), regardless of ice giant growth timescales. However, when the gas surface density exceeds ~10 g/cm^2 in the 10-20 au range, inward Type-I migration of ice giant embryos occurs due to angular momentum exchange with the disk (Ward 1997; Izidoro et al. 2015). This migration, especially in the 'wide' planetary configuration, causes Uranus and Neptune to spiral inward, sometimes reaching 12 au. Rapid planet formation ($\tau_{\rm growth} = 1 \times 10^5$ yr) amplifies this effect, rapidly redistributing planetesimals toward the asteroid belt. By 300 kyr, over half of the implanted objects come from beyond 10 au, indicating that migration, rather than planetary growth, is the primary driver of implantation. However, despite varied origins, the final asteroid belt distribution is similar to that of Saturn-region objects, with a slight shift toward lower heliocentric distances. Ice giant migration is crucial for achieving the 1.1:1 CI/CM ratio observed today.

We find that the most influential factor for the distribution of objects within the asteroid belt proves to be the gas profile of the protoplanetary disk. The final distribution of objects successfully implanted in the asteroid belt mirrors the shape of the gas profile. We tested our hypothesis further by simulating pressure bumps within the protoplanetary disk, by introducing gas profiles characterized by Gaussian peaks. We find that bodies formed around Saturn will be implanted with the same radial distribution as those that originate around Neptune. Whatever the gas profile, it is interesting to note a small inward radial shift of implanted bodies relative to the gas distribution.

We used a Kolmogorov-Smirnov (KS) test to compare the semi-major axis distributions of our final popu-

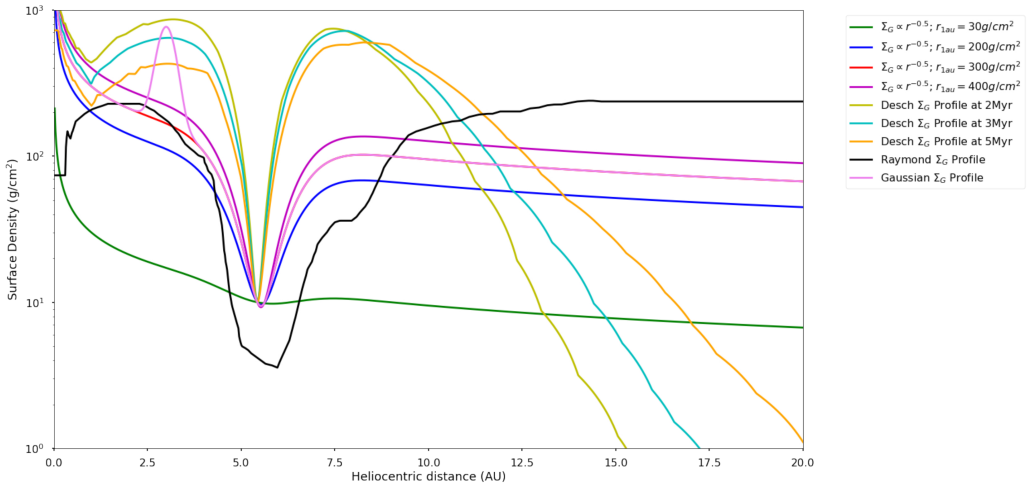

Fig. 2. Gas profiles used in our simulations. We assumed Jupiter had opened a gap in the gaseous disk at approximately 5.4 au. The Gaussian profile allows us to create a pressure trap in a targeted region.

lations with observed CM-like bodies. The best-fitting simulation involved forcing a Gaussian pressure bump at 3.0 au, suggesting a planetesimal trap in this region during CM implantation, likely during Saturn's growth. This pressure bump could result from buildup around the water ice line, which was near 3.0 au around 1 Myr after CAIs (Schneeberger, Antoine et al. 2023), although CM chondrites formed 3-4 Myrs later, when the ice line may have shifted (Aguichine et al. 2022; Lichtenberg et al. 2021). Alternatively, it could represent the inner edge of Jupiter's gap, implying the CM distribution reflects Jupiter's gap at the time of implantation. No gas profiles from the literature could replicate the asymmetric CI-like body distribution.

4 Conclusion

Our numerical simulations suggest that the distribution of small bodies implanted in the asteroid belt reflects the protoplanetary disk's gas profile at the time of implantation. This implies that CM and CI chondrites were not implanted simultaneously. If they were, we would expect similar distributions, yet their distinct profiles point to a time lag between their formation and implantation. This highlights that the timing of their ejection from their formation zones, rather than their initial location (e.g., 10 au vs. 20 au), plays a critical role in determining their final distribution in the asteroid belt.

CM chondrites likely formed in Saturn's region, becoming implanted during Saturn's growth phase, shaped by Jupiter's gap. In contrast, CI chondrites and IDP-like P/D-types were implanted later, after Uranus and Neptune's growth and migration when the gas profile was largely depleted. This timing difference explains the asymmetric distribution of CI-like bodies.

A notable challenge is reproducing the similar eccentricity and inclination distributions of CI- and CM-like bodies, which our simulations did not capture. This suggests a post-implantation event, such as Jupiter's jump from 5.4 to 5.2 au, that could have excited objects and reduced the population beyond Jupiter's 2:1 resonance.

These findings also provide insights into chondrule formation. CM chondrites, rich in chondrules, likely formed in Saturn's region, while the chondrule-free CI chondrites originated at a higher heliocentric distance. This points to chondrule formation occurring predominantly inward of the ice giants, with increasing efficiency closer to the Sun, a factor future models must incorporate.

Lastly, our simulations indicate that CM-like planetesimals were a primary source of Earth's water, with up to 1.5% of CM-like bodies reaching the terrestrial zone. This aligns with Earth's ocean and mantle water content, as well as its D/H ratio. In contrast, the contribution of CI-like planetesimals was negligible due to their late implantation after gas dispersal.

Our study also demonstrates a critical bias in all dynamical models of the early Solar System, as they typically assume a single gas profile.

References

Aguichine, A., Mousis, O., & Lunine, J. I. 2022, Planet. Sci. J., 3, 141

Bitsch, B., Johansen, A., Lambrechts, M., & Morbidelli, A. 2015, A&A, 575, A28

Cresswell, P. & Nelson, R. P. 2008, A&A, 482, 677

Deienno, R., Morbidelli, A., Gomes, R. S., & Nesvorný, D. 2017, AJ, 153, 153

Desch, S. J., Kalyaan, A., & Alexander, C. M. O. 2018, The Astrophysical Journal Supplement Series, 238, 11

Gomes, R. S. 2003, Icarus, 161, 404

Hopp, T., Dauphas, N., Abe, Y., et al. 2022, Science Advances, 8, eadd8141

Izidoro, A., Dasgupta, R., Raymond, S. N., et al. 2022, Nature Astronomy, 6, 357

Izidoro, A., Morbidelli, A., Raymond, S. N., Hersant, F., & Pierens, A. 2015, A&A, 582, A99

Kaib, N. A. & Quinn, T. 2008, Icarus, 197, 221

Kobayashi, H., Ormel, C. W., & Ida, S. 2012, The Astrophysical Journal, 756, 70

Lambrechts, M., Johansen, A., & Morbidelli, A. 2014, A&A, 572, A35

Levison, H. F., Morbidelli, A., Vanlaerhoven, C., Gomes, R., & Tsiganis, K. 2008, Icarus, 196, 258

Lichtenberg, T., Drażkowska, J., Schönbächler, M., Golabek, G. J., & Hands, T. O. 2021, Science, 371, 365

Morbidelli, A., Levison, H. F., Tsiganis, K., & Gomes, R. 2005, Nature, 435, 462

Nesvorný, D. 2015, The Astronomical Journal, 150, 73

Raymond, S. N. & Izidoro, A. 2017, Science Advances, 3, e1701138

Raymond, S. N. & Izidoro, A. 2017, Icarus, 297, 134

Rein, H. & Liu, S. F. 2012, A&A, 537, A128
Ronnet, T., Mousis, O., & Vernazza, P. 2017, The Astrophysical Journal, 845, 92
Ronnet, T., Mousis, O., Vernazza, P., Lunine, J. I., & Crida, A. 2018, AJ, 155, 224
Schneeberger, Antoine, Mousis, Olivier, Aguichine, Artyom, & Lunine, Jonathan I. 2023, A&A, 670, A28
Shakura, N. I. & Sunyaev, R. A. 1973, A&A, 24, 337
Tsiganis, K., Gomes, R., Morbidelli, A., & Levison, H. F. 2005, Nature, 435, 459
Vernazza, P., Ferrais, M., Jorda, L., et al. 2021, A&A, 654, A56
Walsh, K. J., Morbidelli, A., Raymond, S. N., O'Brien, D. P., & Mandell, A. M. 2011, Nature, 475, 206
Ward, W. R. 1997, Icarus, 126, 261
Yada, T., Abe, M., Okada, T., et al. 2021, Nature Astronomy, 6, 214
Yokoyama, T., Nagashima, K., Nakai, I., et al. 2023, Science, 379, eabn7850